A multichannel, real-time MRI RF power monitor for independent SAR determination

AbdEl-Monem M. El-Sharkawy[a)]
Russell H. Morgan Department of Radiology and Radiological Science, Johns Hopkins, University School of Medicine, Baltimore, Maryland 21287

Di Qian and Paul A. Bottomley
Russell H. Morgan Department of Radiology and Radiological Science, Johns Hopkins, University School of Medicine, Baltimore, Maryland 21287 and Department of Electrical and Computer Engineering, Johns Hopkins University, Baltimore, Maryland 21287

William A. Edelstein
Russell H. Morgan Department of Radiology and Radiological Science, Johns Hopkins, University School of Medicine, Baltimore, Maryland 21287

(Received 21 September 2011; revised 5 March 2012; accepted for publication 9 March 2012; published 11 April 2012)

Purpose: Accurate measurements of the RF power delivered during clinical MRI are essential for safety and regulatory compliance, avoiding inappropriate restrictions on clinical MRI sequences, and for testing the MRI safety of peripheral and interventional devices at known RF exposure levels. The goal is to make independent RF power measurements to test the accuracy of scanner-reported specific absorption rate (SAR) over the extraordinary range of operating conditions routinely encountered in MRI.
Methods: A six channel, high dynamic range, real-time power profiling system was designed and built for monitoring power delivery during MRI up to 440 MHz. The system was calibrated and used in two 3 T scanners to measure power applied to human subjects during MRI scans. The results were compared with the scanner-reported SAR.
Results: The new power measurement system has highly linear performance over a 90 dB dynamic range and a wide range of MRI duty cycles. It has about 0.1 dB insertion loss that does not interfere with scanner operation. The measurements of whole-body SAR in volunteers showed that scanner-reported SAR was significantly overestimated by up to about 2.2 fold.
Conclusions: The new power monitor system can accurately and independently measure RF power deposition over the wide range of conditions routinely encountered during MRI. Scanner-reported SAR values are not appropriate for setting exposure limits during device or pulse sequence testing.
 [http://dx.doi.org/10.1118/1.3700169]

Key words: power monitoring, RF safety, SAR, heating

I. INTRODUCTION

Accurate knowledge of the RF specific absorption rate (SAR) in the body during MRI scans is important for patient safety and compliance with limits mandated by the Food and Drug Administration (FDA) in the USA (Ref. 1) and the International Electrotechnical Commission (IEC) in Europe.[2] In addition to ensuring safe operation and regulatory compliance, accurate power monitoring can avoid restrictions on clinical MRI sequences arising from incorrect estimation of the delivered power. Accurate knowledge of delivered power is essential for testing the MRI safety of peripheral, implanted and interventional devices at defined RF exposure levels.[3–6]

RF safety concerns initially arose with the introduction of higher-field 1.5 T whole-body MRI scanners and the recognition that SAR increases approximately with the square of MRI frequency or field strength when other MRI sequence parameters are kept constant.[7–9] The recent emergence of clinical 3 T scanners and experimental body systems operating at 7 T and higher,[10] in which SAR could potentially increase 4-fold to more than 20-fold compared to 1.5 T, only exacerbates concerns about safety and how to ensure compliance with SAR guidelines.[1,2]

In clinical MRI scanners, SAR monitoring for safety and regulatory compliance is generally carried out by scanner software and hardware that is largely proprietary, with "scanner SAR" values typically logged for each study. These systems prohibit or terminate scanning based on predictions of body SAR relying on internal measures, modeling, and prior characterization or assumed properties of the MRI transmit coil. Electromagnetic modeling with knowledge of the input power[11–13] and thermal mapping[14,15] can help provide a detailed understanding of whole-body and local SAR. Yet, rare as they may be compared to the total number of MRI scans performed, RF burns do occur, a fraction of which are reported to the FDA.[16] In these cases at least, a failure in scanner SAR monitoring has occurred.

Unfortunately, investigating whether the scanner is operating safely within SAR guidelines by means that are

independent of the scanner, if performed at all, is not easy.[17] The accuracy of scanner SAR estimates is also questionable in light of discrepancies with thermally derived SAR measurements,[17,18] especially during MRI safety testing of interventional devices[3,18–20] and the lack of correlation between subjective heat perception by patients and scanner SAR.[21]

Setting precise SAR exposure levels for investigators testing devices or MRI methods, or for evaluating SAR in individual burn cases,[22] requires accurate and independent measurement tools. This starts with accurate measurements of the total power deposited and requires a reliable RF power meter. The RF power monitors built into the MRI scanner are usually attached to the RF power amplifier output. However, measuring the power delivered to the body is complicated by losses in the RF transmission chain, including the cables, switches, the quadrature-hybrid (Q-hybrid) and the MRI coil.[23,24] These losses can vary over time, but are not routinely monitored.

Moreover, as we now report, the very high dynamic range (DR = peak-to-average power ratio) of RF transmit pulses, and MRI duty cycles that span orders-of-magnitude, are beyond the capabilities of available commercial power meters.[25] The meters are usually adequate for pulse sequences with short repetition periods (TR) and consistent high-power levels. However, they typically do not give accurate results for sequences using mixtures of high and low amplitudes or modulations, or long TR.

We have therefore developed a high-DR, MRI-compatible, power profiling system for measuring and recording RF power over a wide range of MRI scan conditions. The system is broadband up to 440 MHz, can be used to sample power for both local and whole-body power flow, and unlike commercial meters, has six channels and a buffer size suitable for monitoring power at multiple locations over extended time periods. We report its application to real-time RF power monitoring in human whole-body MRI studies of volunteers performed in commercial Philips Medical Systems' (Best, The Netherlands) and Siemens Medical Solutions' (Malvern, PA) 3 T MRI scanners. We show that the actual power deposited and the body-average SAR,[1,2] often vary considerably from the scanners' own estimates.

II. METHODS

II.A. RF power measurement

The losses in the RF power chain of a Philips 3 T *Achieva* XMR scanner[26] were first characterized using a 4395 A Agilent Technologies (Santa Clara, CA) network analyzer by measuring the attenuation in each stage in accordance with the schematic in Fig. 1. Measured losses in these components show that the power output at the Q-hybrid (points D, E, Fig. 1) is only about 59% of the power out of the RF amplifier (point A).

To measure the pulse power during MRI, we first tried commercial inline power meters. Bird 5014 and Bird 5010 b (*Bird Technologies, Solon, OH*) did not work correctly for peak/average power ratios greater than ten. Even when operating the scanner at minimum TRs and low RF field intensity (B_1), measurements were unstable and irreproducible.

We next used a Ladybug Technologies LLC (Santa Rosa, CA), LB480A power profiling meter in combination with 50 dB dual directional couplers to measure forward and reverse power at the outputs of the power amplifier and the Q-hybrid during MRI. The Ladybug meter sampled the pulse profile at 10 μs intervals and stored results for power calculations. While this yielded accurate measurements on four volunteers,[27] the use of USB cables from Ladybug to the computer necessitated a person inside the scanner room. Moreover, the Ladybug meter did not have sufficient channels for monitoring the forward and reverse power at the three locations of interest simultaneously [A, D, and E in Fig. 1(a)]. In addition, its small buffer size ($\leq$1 s) was inadequate for providing continuous measurements of power for many MRI sequences with long TRs over the several cycles needed for accurately measuring time-averaged power, thus rendering real-time measurements impractical.

We therefore built a six-channel scanner-independent power monitoring system. This used six power sensor circuits [PSC, Fig. 2(a)] assembled from AD8310 logarithmic amplifier IC's (Analog Devices, Norwood MA). At each of three locations (RF amplifier output, two Q-hybrid outputs), a power profiling measurement module (PPMM) consisting of a 50 dB directional coupler (Werlatone, Inc., Patterson NY) connected to two PSCs, one to its forward channel and one to its reverse channel [Fig. 2(b)], was deployed. A10 dB attenuator was added to the forward channels to allow measurements of up to 50 kW of peak power. The design DR was from 17 dBm (nearly the maximum input power of the AD8310) to −80 dBm over the desired frequency range 1–440 MHz. Each PSC is powered by a rechargeable lithium ion, nonmagnetic 4 V battery (PowerStream, Orem UT) and can operate continuously for at least 10 h before recharging. The video bandwidth of the ICs was set to ~112 KHz using a 470 PF capacitor [Fig. 2(a)].

The outputs of each of the six PSCs are simultaneously sampled in differential input mode at 200 kHz by a 16 bit USB-6251 National Instruments (Austin, TX) data acquisition system controlled by a laptop computer that also stores the power measurement data. The 5 μs sampling resolution accurately captures the MRI RF pulse modulation whose

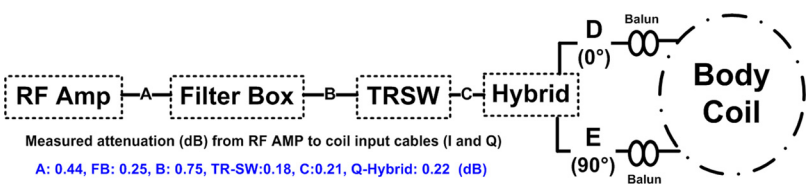

FIG. 1. Schematic of the Philips Achieva RF power delivery chain. Shown are the RF amplifier (RF AMP), measured cable attenuations in dB (A, B, C), the filter box (FB) penetrating the scanner's Faraday cage, the transmit switch (TRSW) and the Q-hybrid outputs (D, E).

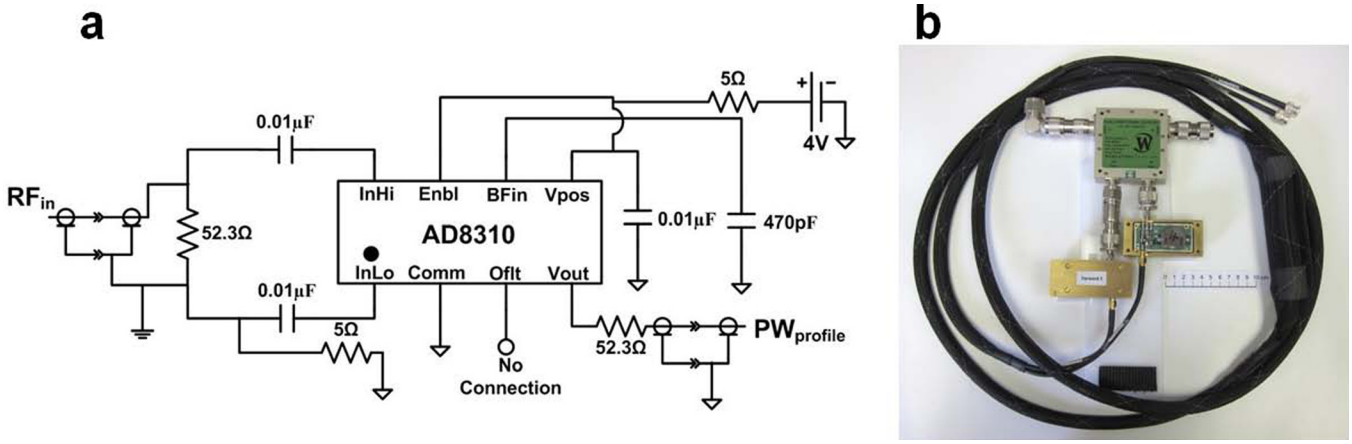

FIG. 2. (a) Circuit diagram of the digital power sensor circuit (PSC) based on the AD8310 IC. (b) Picture of one of the three power profiling measurement modules (PPMM) showing the directional coupler and PSCs.

time resolution in the Philips scanner was about 6.4 μs. A MATLAB (The Mathworks, Natick, MA) program was written to read the saved voltage files, convert them to power profiles using the linear calibration curves for each channel, and to calculate average power values for all experiments. A schematic of the system configured to monitor RF power flow is shown in Fig. 3. The (low frequency) power profiling lines from the PPMMs attached to the quad hybrid outputs are fed through the scanner room's connection panel. The lines from the PPMM connected to the RF power amplifier were wound around ferrite cores to prevent RF interference.

Each PPMM was bench calibrated for the operational frequencies of the Philips 3 T Achieva scanner and a Siemens 3 T Trio scanner (127.8 and 123 MHz, respectively) using the setup shown in Fig. 4(a). The calibration was performed against the LB480A meter using a 10 dBm frequency synthesizer whose output was connected to a 0–100 dB variable attenuator to vary the input power level. The PSC voltage-to-logarithmic power was measured over a 70 dB range (limited by the LB480A unit's operational dynamic range) and was highly linear as shown in Fig. 4(b). The slopes of the calibration curves were about 0.24 V/10 dBm. The net sampling resolution of the A/D was set to 0.004 dBm. After calibration the full DR was tested over a range of 90 dB as shown in Fig. 4(c) and exhibited a maximum deviation of 0.8 dBm from linearity at −80 dBm. The total insertion loss of the monitoring system PPMMs at 128 MHz was 0.1 dB or about 2%.

II.B. RF Power Deposition

Figure 5 shows a schematic resonant circuit for an MRI coil producing a transmit RF field, B_1, proportional to the current, I, in the coil. The power loss in the circuit is the sum of the coil and subject losses in resistive loads R_C and R_S, respectively. The pickup loops, are fixed by the manufacturer inside the RF body coil. They are used by the scanner to monitor and set the initial value of the RF field produced by the coil during set-up. The power loss in the coil P_{coil}, is measured as the net power flow at the output of the Q-hybrid with a lossless sample placed in the coil. The lossless sample is a 1 l bottle of mineral oil whose RF dielectric constant,

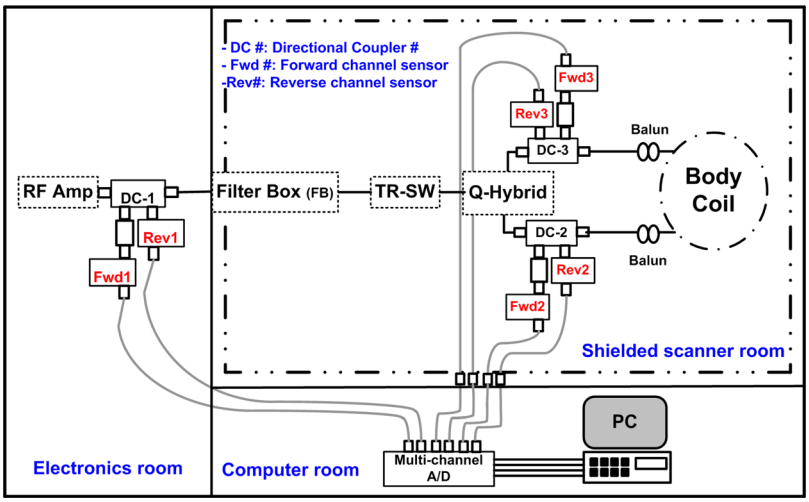

FIG. 3. Schematic of the power measurement setup where DC-1, Fwd1 and Rev1 are directional coupler, forward channel 1 sensor and reverse channel 1 sensor respectively, etc.

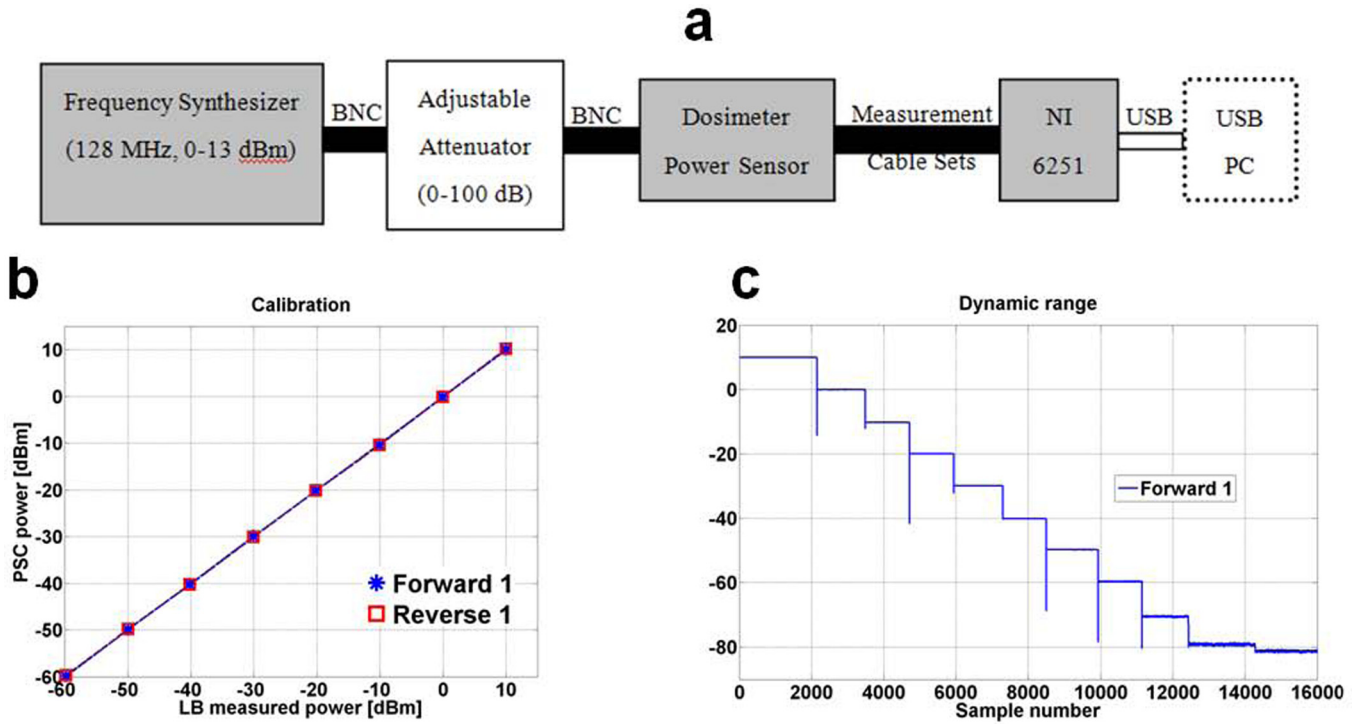

FIG. 4. (a) Bench setup for calibrating PSC units as well as testing dynamic range and linear performance. NI 6251 is the National Instruments data acquisition system. (b) Calibration curve, PSC vs Ladybug meter showing linearity, (c) PSC 90 dB dynamic range.

conductivity and size are orders-of-magnitude lower than those of the body.[28,29] This was verified by measuring P_{coil} with additional mineral oil sample volumes of 2 and 3 l; no significant change in power absorption was observed. The desired B_1, and therefore the current I required to produce it, is approximately constant, independent of the subject being imaged.[30,31] Therefore the coil power dissipation, P_{coil}, is constant for a given pulse sequence, independent of the subject. The power deposited in the subject is then $P_{subject} = P_{total} - P_{coil}$, where P_{total} is the total power dissipated in the coil plus the subject measured at the Q-hybrid. Note that larger subjects have greater P_{total} but the same P_{coil}.

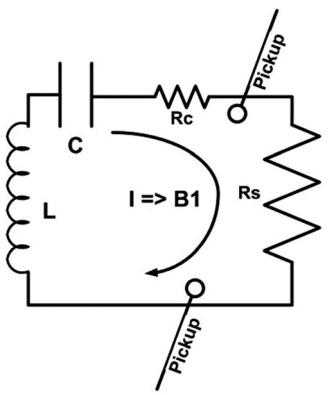

FIG. 5. A schematic resonant circuit for an MRI coil producing a certain B_1 field. Rc is the coil resistance and Rs is the resistance reflected into the coil circuit by the imaging subject load. B_1 is proportional to current I in the coil and Power loss $= I^2 \cdot (Rc + Rs)$. Shown also are pickup loops used by the scanner to monitor the B_1 RF field produced by the coil.

To measure the RF power deposited in human subjects during MRI, the power monitoring system was connected to the output of the RF power amplifier and the two outputs of the Q-hybrid before the scan. Eleven healthy volunteers (9 men, 2 women; age 22–65 yr) were recruited and provided informed consent for this study approved by The Johns Hopkins Institutional Review Board on Human Investigation. Subjects were positioned in the Philips 3 T scanner and the scanner's automated scan preparation sequence initiated. Volunteers were landmarked at the xiphoid, placed at the isocenter of the scanner and a transverse slice was targeted. A reference B_1 RF field is first set based on pickup coil sensors, followed by the scanner's MRI-based B_1 optimization algorithm which sets the final flip angle. The B_1 optimization algorithm is based on a stimulated echo sequence similar to the one described by Akoka *et al.*[32] where an average signal projection is used, thus rendering the result stable against local field variations. Two field-echo (FE) MRI sequences with TR = 50 ms and two different RF pulse shapes (a short 1 ms asymmetric two lobe pulse and a long 7 ms "Spredrex" pulse[33]) were used. The total scanner time per subject—including entry, positioning, and egress from the scanner—was 10–15 min.

The delivered RF power reported by the scanner, as well as the measured power output, was recorded. The subject was replaced by the mineral oil phantom and the pulse sequence repeated to produce the same B_1 detected by the pickup coil. Scanner SAR and power were again recorded, along with the power measured by our power monitoring system. Body-average SAR was taken as the power deposited divided by the subject's weight, in accordance with the standard definition.[1,2]

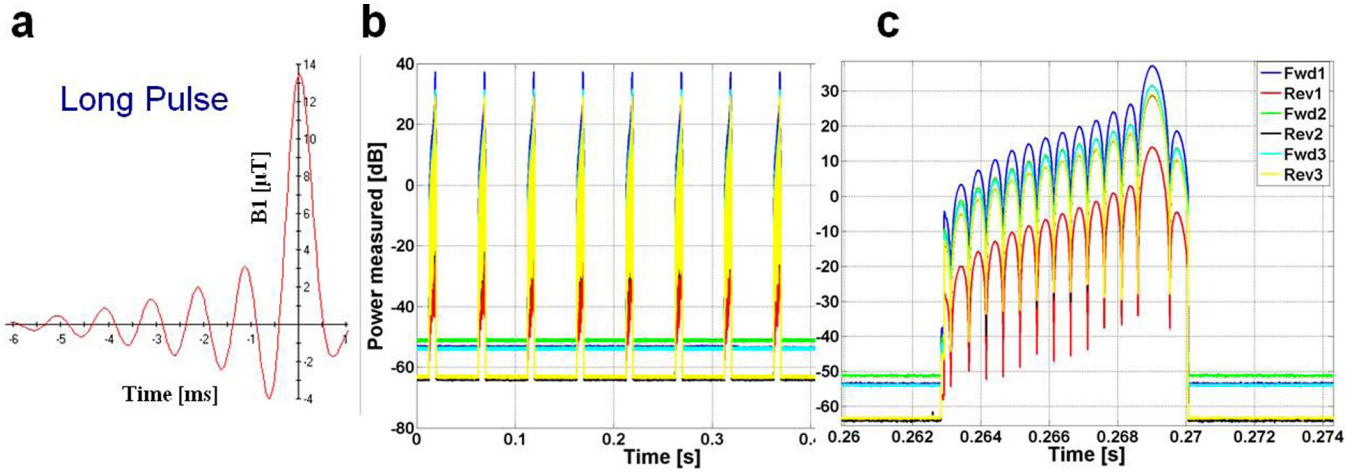

FIG. 6. Real-time profile of a ~7 ms asymmetric, slice selective RF pulse in the Philips scanner. (a) Scanner B_1 linear pulse envelope simulator. (b) Recorded time window of RF power in real-time for long RF pulses. (c) A single pulse (logarithmic scale).

The same protocol was repeated on six of the volunteers (men, age 23–66 yr) in a Siemens 3 T Trio scanner. The FE sequence used the scanner's default ~2 ms RF sinc pulse with one side lobe. The scanner's console SAR differed from the value reported in its log file, so both values were recorded.

All power values measured by our power monitoring system were calculated by averaging instantaneous power over a 0.5 s time window (ten pulses for FE pulse sequence).

III. RESULTS

MRI experiments showed no noticeable interference or image degradation with the PPMMs connected. Connecting the PPMMs did not increase noise, as was confirmed by noise scans acquired with the RF and gradients turned off.

Figure 6 exemplifies the six-channel real-time recordings of an asymmetric, multilobe, slice selective RF pulse on the Philips scanner with a subject present. The detailed instantaneous recording of RF power is shown for Spredrex pulses on a logarithmic scale.[33]

The results for the forward power delivered to the Philips body MRI coil and body-average SAR for all subjects in the Philips scanner are plotted in Fig. 7 as a function of the power reported by the scanner, the patient weight, and the body mass index (BMI). Figure 7(a) shows that the scanner-reported power at the RF amplifier's output agrees with our PPMM system results to within 6% for short pulses (~1 ms). This is not true for longer pulses (~7 ms), where the scanner's RF power monitoring fails when compared to the PPMM system that had been calibrated over the full DR and duty cycles used for MRI. For all volunteers, the power delivered at the output of the Philips Q-hybrid is $56.5 \pm 2.5\%$ of the output of the amplifier. This figure is consistent with the 58.5% predicted from the measured losses in the Philips RF chain plus the measured insertion losses in the power monitoring modules. For the 50 ms TR, the average power dissipated in the coil is 8.8 ± 0.6 W for the short pulses and 11.1 ± 0.8 W for the long pulses, independent of the size of the mineral oil bottle (1–3 l).

The Philips Achieva scanner initially establishes a B_1 that is the same for all samples using pickup loops. It is worth noting that the final MRI optimization yielded a B_1 that was, on average, within 5% of the initial pickup loop B_1 in all samples, from small to large human subjects as well as in the mineral oil bottles. This result supports the assumption that the current I required to produce a desired MRI flip angle across the slice projection is essentially independent of sample size, and that the power dissipation in the RF coil always equals the power dissipation with the mineral oil sample to a good approximation.

Figure 7(b) shows that the measured deposited power varies linearly with BMI with a correlation coefficient $R^2 = 0.8$ (0.7) for the short (the long) RF pulses. Figures 7(c) and 7(d) show that the scanner almost always overestimates body-average SAR. The scanner overestimated SAR by up to 78% (1.8 fold) for short pulses and 123% (2.2 fold) for long pulses when compared to values obtained from our PPMM direct power determination and subject weights.

Figure 8 shows the calculated SAR values from the real-time power monitor versus the scanner-reported values for 3 T Siemens scanner. The power delivered at the output of the Q-hybrid is $90 \pm 2\%$ of the power measured at the RF amplifier output. SAR values listed in the Siemens log file differ from those reported at the console: Siemens does not state which values they use. In any case, as with the Philips scanner, the Siemens scanner frequently overestimated SAR. The Siemens scanner log overestimated SAR by up to 103% (2 fold) while the console values were up to 71% (1.7 fold) above the actual measured SAR.

IV. DISCUSSION

This paper addresses the problem of providing accurate real-time measurements of the RF power delivered to the body, which is inadequately served by existing technology. Specifically, we found that two commonly available commercial RF power meters are unsuitable for the full range of DRs, duty cycles and pulse types encountered in MRI. This was further underscored by differences and errors in power

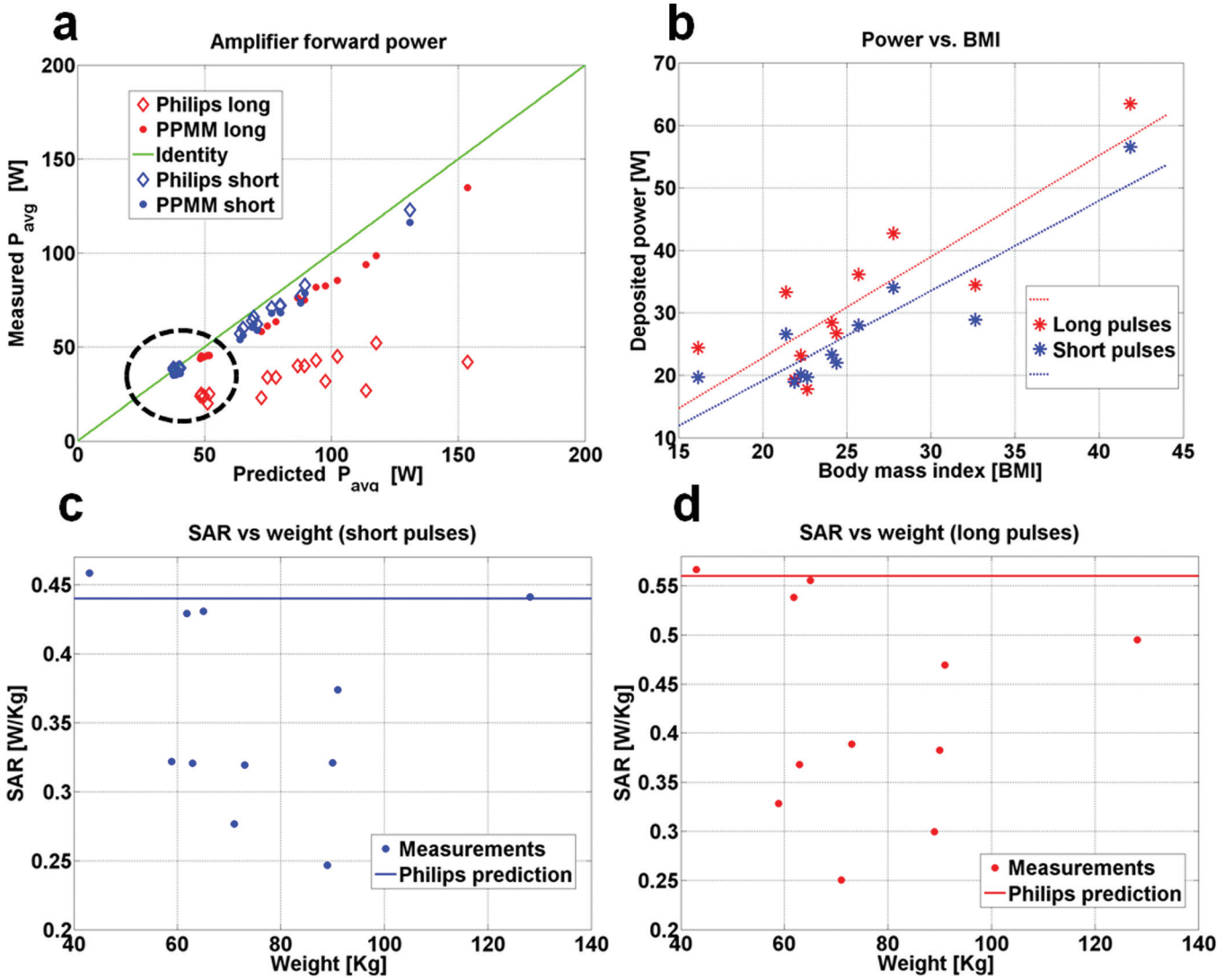

FIG. 7. (a) Philips Achieva amplifier output power measurements using the PPMM (solid circles), and the scanner power monitoring unit (open diamonds, reported in the log file), vs scanner average predicted power. Power data are from 11 human volunteers, plus four measurements from mineral oil bottles (circled), using short (1 ms, blue), and long (7 ms, red) slice selective pulses. The green line represents identity. (b) Total power deposited in the body measured by the PPMM, as a function of BMI. Lines of best fit correspond to long (red) and short (blue) pulses. Also shown is the PPMM-measured whole-body SAR for (c) short and (d) long pulses, as compared to the scanner predicted SAR from scanner log files (horizontal lines).

monitoring for short and long RF pulses in the Philips scanner. We therefore developed a real-time, multichannel power monitoring system suitable for a full range of MRI RF pulses and sequences operating over a frequency range that will accommodate scanners with fields up to 10 T.[34]

The accuracy of measurements provided by our power monitoring system was independently validated three ways: (1) on the bench using the Ladybug power meter (Fig. 4); (2) using the 3 T scanner's power monitoring unit at the output of the amplifier for high-power, short RF pulses [Fig. 7(a)]; and (3) by measuring the losses in the 3 T scanner's RF chain using our power monitor and comparing the results with independent measurements made with a network analyzer.

Our new power monitoring system was used to determine the true power deposited and the body-average SAR delivered to adult volunteers in two clinical 3 T MRI systems. The results showed that the scanners almost always overestimate the body-average SAR as compared to the actual power deposited. The overestimates were as much as 120% (2.2 fold) and 100% (2 fold), respectively, in the Philips and Siemens 3 T systems studied here [Figs. 7(c), 7(d), and 8). Unfortunately, the exact details of the manufacturer's SAR modeling are proprietary, precluding the identification of specific causes for the differences. Nevertheless, the data in Fig. 7 suggest Philips' use of a worst-case estimate that is independent of the subject loading, while Siemens' model seems to depends on the subject's weight (Fig. 8). Although the evaluations were performed on the scanner's whole-body coils with sample-dominant losses, application of the power monitoring system is not limited by coil geometry, and similar measurements could be performed on other vendors' scanners and other coil sets, including multitransmit systems at various field strengths.[34]

The power monitoring system and protocol presented here can only provide measures of the total power deposited in the body during MRI, or the body-average SAR defined as

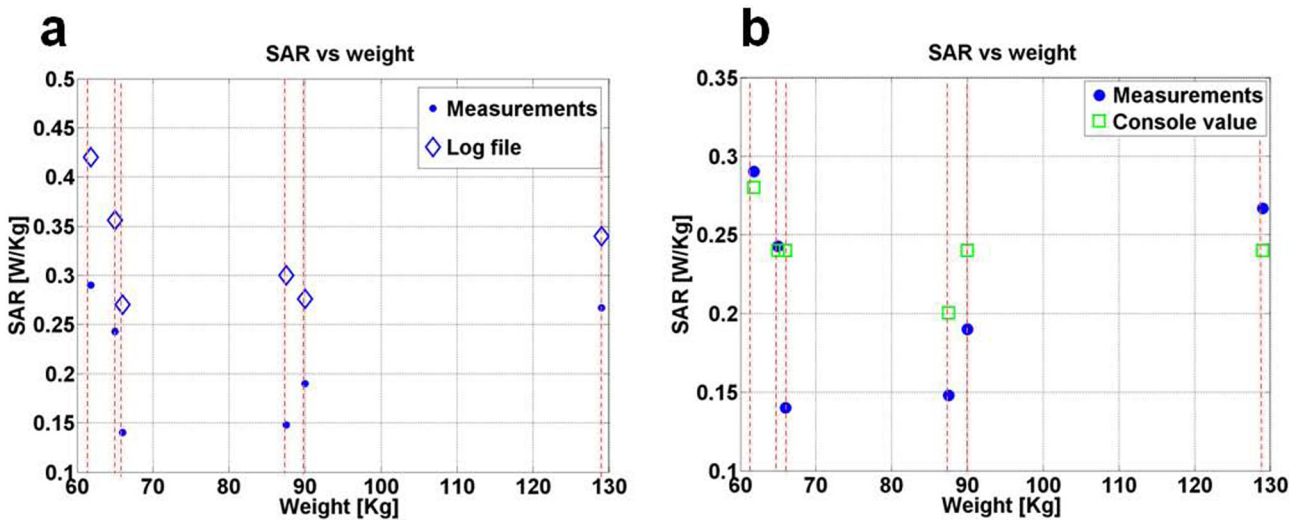

FIG. 8. Measured SAR for six volunteers on the Siemens 3 T system (solid dots) compared to scanner-reported values from (a) the log file and (b) the scanner console.

the total power divided by the subject's weight.[1,2] Local SAR exposure such as peak 1-g or 10-g averages, are also important for safety compliance.[1,2] At present, these must be obtained by numerical electromagnetic modeling,[11–14,35–37] from which ratios of the peak local SAR to the total power can be derived. These are, however, anatomy dependent. In practice, the total deposited power may be used in conjunction with numerical electromagnetic models to provide estimated local SAR values.[17,35–40]

In the Philips scanner, because of losses in the cables, RF coil and other transmit chain components, the power reaching the imaging subject was less than half the power supplied by the RF transmitter. The smaller power loss for the Siemens scanner indicates the use of lower loss components. Moreover, both scanners' whole-body SAR estimates reported to the scanner operator seem conservatively overstated. While this may provide an extra safety margin for RF exposure, it nevertheless means that scanner SAR values are not reliable for specifying RF exposure when testing the MRI safety of peripheral, implanted and interventional devices.[3,20] The overestimate may also limit high-SAR pulse sequences, forcing reductions in duty cycle or pulse power that unnecessarily increase scan time and/or compromise efficiency or performance.

Our power monitoring system requires temporary connections to system hardware to operate. In future, an RF dosimeter with a stand-alone transducer for SAR monitoring[17] is planned for providing scanner-independent SAR measurements without any scanner connections. The dosimeter would employ the system described here for monitoring power in the transducer and for calibrating the deposited power.

In conclusion, we have presented a versatile approach to accurately measure, in real-time, the total RF power deposition during MRI, independent of the scanner. We have used our real-time power monitoring system to demonstrate deficiencies in commercial scanner-reported RF SAR values. Our system can be used to monitor regulatory compliance, SAR dosimetry, evaluation of scanner function following burn injuries and for setting RF exposure levels during device safety testing.

ACKNOWLEDGMENTS

The authors thank *Dr. Michael Schär and Mr. Robert Canoles*, Philips Healthcare, Cleveland, OH, for help with the Achiva Philips 3 T scanner. Supported by NIH R01EB007829.

[a]Author to whom correspondence should be addressed. Electronic mail: abdshark@gmail.com; Telephone: 443-287-7749.

[1]Guidance for Industry and FDA, "Staff criteria for significant risk investigations of magnetic resonance diagnostic devices," United States Food and Drug Administration (FDA), 2003.
[2]Medical electrical equipment—Part 2-33, "Particular requirements for the safety of magnetic resonance equipment for medical diagnosis," European Committee for Electrotechnical Standardization Central Secretariat, IEC Report No. 60601-2-33 (2002).
[3]P. A. Bottomley, A. Kumar, W. A. Edelstein, J. M. Allen, and P. V. Karmarkar, "Designing passive MRI-safe implantable conducting leads with electrodes," Med. Phys. **37**, 3828–3843 (2010).
[4]E. Mattei, G. Calcagnini, M. Triventi, F. Censi, P. Bartolini, W. Kainz, and H. Bassen, "MRI induced heating of pacemaker leads: Effect of temperature probe positioning and pacemaker placement on lead tip heating and local SAR," Conf. Proc. IEEE Eng. Med. Biol. Soc. **2006**, 1889–1892 (2006).
[5]H. Muranaka, T. Horiguchi, S. Usui, Y. Ueda, O. Nakamura, and F. Ikeda, "Dependence of RF heating on SAR and implant position in a 1.5T MR system," Magn. Reson. Med. Sci. **6**, 199–209 (2007).
[6]W. R. Nitz, G. Brinker, D. Diehl, and G. Frese, "Specific absorption rate as a poor indicator of magnetic resonance-related implant heating," Invest. Radiol. **40**, 773–776 (2005).
[7]P. A. Bottomley and E. R. Andrew, "RF magnetic field penetration, phase-shift and power dissipation in biological tissue: Implications for NMR Imaging," Phys. Med. Biol. **23**, 630–643 (1978).
[8]P. A. Bottomley, R. W. Redington, W. A. Edelstein, and J. F. Schenck, "Estimating radiofrequency power deposition in body NMR imaging," Magn. Reson. Med. **2**, 336–349 (1985).
[9]P. A. Bottomley and W. A. Edelstein, "Power deposition in whole-body NMR imaging," Med. Phys. **8**, 510–512 (1981).
[10]C. Wang, G. X. Shen, J. Yuan, P. Qu, and B. Wu, "Theoretical and experimental investigation of the relationship among SAR, tissues and radio frequencies in MRI," Phys. Med. **21**, 61–64 (2005).
[11]C. M. Collins and Z. Wang, "Calculation of radiofrequency electromagnetic fields and their effects in MRI of human subjects," Magn. Reson. Med. **65**, 1470–1482 (2011).

[12]H. Homann, P. Börnert, H. Eggers, K. Nehrke, O. Dössel, and I. Graesslin, "Toward individualized SAR models and in vivo validation," Magn. Reson. Med. **66**, 1767–1776 (2011).
[13]Z. Wang, J. C. Lin, W. Mao, W. Liu, M. B. Smith, and C. M. Collins, "SAR and temperature: Simulations and comparison to regulatory limits for MRI," J. Magn. Reson. Imaging **26**, 437–441 (2007).
[14]S. Oh, A. G. Webb, T. Neuberger, B. Park, and C. M. Collins, "Experimental and numerical assessment of MRI-induced temperature change and SAR distributions in phantoms and in vivo," Magn. Reson. Med. **63**, 218–223 (2010).
[15]P. Ehses, F. Fidler, P. Nordbeck, E. D. Pracht, M. Warmuth, P. M. Jakob, and W. R. Bauer, "MRI thermometry: Fast mapping of RF-induced heating along conductive wires," Magn. Reson. Med. **60**, 457–461 (2008).
[16]"U.S. Food and Drug Administration, Center for Devices and Radiological Health, MAUDE data base reports of adverse events involving medical devices, (http://www.accessdata.fda.gov/scripts/cdrh/cfdocs/cfMAUDE/TextSearch.cfm). Simple search with search term: Magnetic resonance, then screen individual entries for RF burn injuries."
[17]J. P. Stralka and P. A. Bottomley, "A prototype RF dosimeter for independent measurement of the average specific absorption rate (SAR) during MRI," J. Magn. Reson. Imaging **26**, 1296–1302 (2007).
[18]F. G. Shellock, "Comments on MR heating tests of critical implants," J. Magn. Reson. Imaging **26**, 1182–1185 (2007).
[19]A. M. El-Sharkawy, D. Qian, and P. A. Bottomley, "The performance of interventional loopless MRI antennae at higher magnetic field strengths," Med. Phys. **35**, 1995–2006 (2008).
[20]K. B. Baker, J. A. Tkach, J. A. Nyenhuis, M. Phillips, F. G. Shellock, J. Gonzalez-Martinez, and A. R. Rezai, "Evaluation of specific absorption rate as a dosimeter of MRI-related implant heating," J. Magn. Reson. Imaging **20**, 315–320 (2004).
[21]G. Brix, M. Reinl, and G. Brinker, "Sampling and evaluation of specific absorption rates during patient examinations performed on 1.5-Tesla MR systems," Magn. Reson. Imaging **19**, 769–779 (2001).
[22]P. A. Bottomley, "Turning up the heat on MRI," J. Am. Coll. Radiol. **5**, 853–855 (2008).
[23]W. A. Edelstein, G. H. Glover, C. J. Hardy, and R. W. Redington, "The intrinsic signal-to-noise ratio in NMR imaging," Magn. Reson. Med. **3**, 604–618 (1986).
[24]A. Kumar, W. A. Edelstein, and P. A. Bottomley, "Noise figure limits for circular loop MR coils," Magn. Reson. Med. **61**, 1201–1209 (2009).
[25]A. El-Sharkawy, D. Qian, A. Bottomley, and W. Edelstein, "A Multichannel, high dynamic range, real time RF power deposition monitor," Proc. Intl. Soc. Mag. Reson. Med. **19**, 496 (2011).
[26]W. Edelstein, "Radiofrequency Systems and Coils for MRI and MRS," *in Methods in Biomedical Magnetic Resonance Imaging and Spectroscopy*, Vol. 1 (Wiley, New York, NY, 2000), pp. 131–135.
[27]A. El-Sharkawy, D. Qian, A. Bottomley, and W. Edelstein, "Accurate measurement of RF power deposition during 3T MRI," Proc. Intl. Soc. Mag. Reson. Med. **18**, 3853 (2010).
[28]L. Zaremba, "FDA Guidelines for Magnetic Resonance Equipment Safety," Proc. American Ass. of Phys. in Med. (AAPM) **44**, 14–18 (2002).
[29]T. S. Ibrahim, A. M. Abduljalil, B. A. Baertlein, R. Lee, and P. M. L. Robitaille, "Analysis of B_1 field profiles and SAR values for multi-strut transverse electromagnetic RF coils in high field MRI applications," Phys. Med. Biol. **46**, 2545–2555 (2001).
[30]W. A. Edelstein, O. M. Mueller, R. Frey, and D. Vatis, "Electronic method for eliminating prescanning RF transmitter amplitude adjustment," *Society of Magnetic Resonance in Medicine Sixth Annual Meeting*, p. 372, New York, NY (1987).
[31]T. S. Ibrahim, R. Lee, A. M. Abduljalil, B. A. Baertlein, and P. M. Robitaille, "Dielectric resonances and B(1) field inhomogeneity in UHFMRI: Computational analysis and experimental findings," Magn. Reson. Imaging **19**, 219–226 (2001).
[32]S. Akoka, F. Franconi, F. Seguin, and A. Le Pape, "Radiofrequency map of an NMR coil by imaging," Magn. Reson. Imaging **11**, 437–441 (1993).
[33]M. Schar, E. J. Vonken, and M. Stuber, "Simultaneous B(0)- and B(1)+map acquisition for fast localized shim, frequency, and RF power determination in the heart at 3 T," Magn. Reson. Med. **63**, 419–426 (2010).
[34]E. Weber, B. K. Li, F. Liu, and S. Crozier, "A ultra high field multi-element transceiver volume array for small animal MRI," Conf. Proc. IEEE Eng. Med. Biol. Soc. **2008**, 2039–2042 (2008).
[35]P. A. Bottomley and P. B. Roemer, "Homogeneous tissue model estimates of RF power deposition in human NMR studies—Local elevations predicted in surface coil decoupling," Ann. N.Y. Acad. Sci. **649**, 144–159 (1992).
[36]D. Simunic, "Calculation of energy absorption in a human body model in a homogeneous pulsed high-frequency field," Bioelectrochem. Bioenerg. **47**, 221–230 (1998).
[37]W. Liu, C. M. Collins, and M. B. Smith, "Calculations of B-1 distribution, specific energy absorption rate, and intrinsic signal-to-noise ratio for a body-size birdcage coil loaded with different human subjects at 64 and 128 MHz," Appl. Magn. Reson. **29**, 5–18 (2005).
[38]C. M. Collins, S. Li, and M. B. Smith, "SAR and B_1 field distributions in a heterogeneous human head model within a birdcage coil. Specific energy absorption rate," Magn. Reson. Med. **40**, 847–856 (1998).
[39]C. M. Collins, W. Liu, J. Wang, R. Gruetter, J. T. Vaughan, K. Ugurbil, and M. B. Smith, "Temperature and SAR calculations for a human head within volume and surface coils at 64 and 300 MHz," J. Magn. Reson. Imaging **19**, 650–656 (2004).
[40]U. D. Nguyen, J. S. Brown, I. A. Chang, J. Krycia, and M. S. Mirotznik, "Numerical evaluation of heating of the human head due to magnetic resonance imaging," IEEE Trans. Biomed. Eng. **51**, 1301–1309 (2004).